LOW- AND HIGH-CYCLE FATIGUE BEHAVIOUR OF LOAD-CARRYING CRUCIFORM JOINTS CONTAINING INCOMPLETE PENETRATION AND STRENGTH MISMATCH

T. Hanji, C. Miki and K. Saiprasertkit

ABSTRACT

This study investigated the low- and high-cycle fatigue strength of load-carrying cruciform joints containing incomplete penetration and strength mismatch between base metal and weld deposit, and proposed an assessment method based on the local approach. Low- and high-cycle fatigue tests were performed on specimens with varying mismatch and sizes of incomplete penetration. The test results revealed that the crack initiation life was extremely small for this type of joint. In fractographs, dimples observed around the crack initiation site provided evidence of ductile crack propagation. Also, it was found that strength mismatch had a negligible effect on the high-cycle fatigue strength but that under-matching reduced the low-cycle fatigue region. However, a unique relationship was found between local strain around a weld root tip calculated by elasto-plastic finite element analysis and both the low- and high-cycle fatigue life of the specimen.

IIW-Thesaurus keywords: Cruciform Joints; Load-carrying; Low cycle fatigue; Mismatch; Penetration defects; Strength; Thermal cycling.

1 Introduction

The fatigue strengths of welded joints can be reduced as a result of the presence of welding defects. In this respect, existing beam-to-column connections of steel bridge bents, which are widely used in elevated highways in urban areas of Japan, have been found to contain internal flaws in the form of incomplete penetration [1], even though the connections were designed to be fabricated with full penetration welds. An incomplete penetration flaw is a crack-like notch which can be a trigger of fatigue damage due to its high stress concentration. There are two types of possible fatigue damage at these connections during service, high-cycle fatigue damage due to traffic loads [2] and low-cycle fatigue damage due to seismic loads [3]. Therefore, the fatigue strength of the connection needs to be carefully investigated, with respect to both low- and high-cycle fatigue, corresponding to the fatigue lives ranging from tens to millions of applied load cycles.

As illustrated in Figure 1, the existing beam-to-column connections can be identified as load-carrying cruciform joints with incomplete penetration. Extensive research has been conducted on the high-cycle fatigue performance of such cruciform joints [4-9]. On the other hand, only limited studies have been performed on the low-cycle fatigue strength of defective welded joints [10-12], and then mainly focused on butt-welded joints.

High-strength steels are widely used for steel bents, leading to strength under-match between the weld deposit and the base metal, the yield strength of the weld deposit being lower than that of the base metal. The effect of strength mismatch will become a crucial issue when such joints are subjected to high-intensity stress due to extreme loads such as from earthquakes [13-15]. The behaviour of the joints will depend on the strength matching conditions

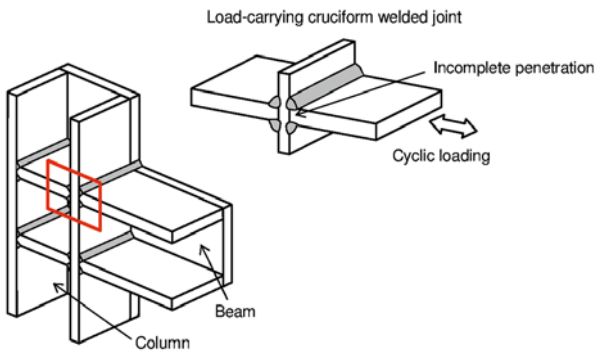

Figure 1 – Load-carrying cruciform joint containing incomplete penetration

Doc. IIW-2204, recommended for publication by Commission XIII "Fatigue of Welded Components and Structures."

since plastic deformation will concentrate in the lower-strength material.

In this study, the fatigue strength of incomplete weld penetration load-carrying cruciform joints with varying degrees of weld-to-base metal strength mismatch was investigated on the basis of both low- and high-cycle fatigue tests. In addition, a local approach was used to assess the fatigue strength of the specimen, based on the local strain around the fatigue crack initiation site calculated by elasto-plastic finite element analysis.

2 Test specimens

2.1 Fabrication

The specimen design is shown in Figure 2. The specimens were made from JIS SM490 or JIS SBHS500 steel, with plate thicknesses of 28 mm and 24 mm, respectively. JIS SBHS500 is a high performance steel with a yield strength of more than 500 MPa.

Two types of specimen, FL and PJP, were fabricated from SM490 steel. Specimen type FL was fabricated with fillet welds, while partial joint penetration groove welds were applied to specimen type PJP. The penetration ratio, defined as the ratio between the length of unfused portion and the thickness of the loaded plate, was designed to be 100 % in FL and 60 % in PJP joints, as shown in Figure 2. Only specimen type FL was produced in the SBHS500 steel. Weld root gaps were set to be almost zero in all specimens.

The welding conditions are given in Table 1. In order to obtain several types of strength matching conditions, different filler materials and shielding gases were selected, based on yield strengths quoted in the welding wire catalogues. SM490 specimens were fabricated to achieve two kinds of under-matching joints and one over-matching

Table 1 – Welding conditions

Index	Welding wires and shield gases (in catalogue)			Welding conditions				
	Type	Diameter [mm]	Yield strength [MPa]	Current [A]	Voltage [V]	Speed [mm/min]	Heat input [kJ/mm]	Interpass temperature [°C]
1	YM-24S + Ar + 40 % CO_2	1.2	380	280 ~ 300	30 ~ 32	250 ~ 300	1.7 ~ 2.1	≤ 50
2	YM-24S + Ar + 10 % CO_2	1.2	380	280 ~ 300	31 ~ 33	240 ~ 300	2.0 ~ 2.4	≤ 50
3	YM-28S + Ar + 20 % CO_2	1.2	480	280 ~ 290	33	270	2.1	≤ 50
4	YM-28 + CO_2	1.2	450	250 ~ 270	26 ~ 28	330 ~ 380	1.1 ~ 1.3	≤ 50

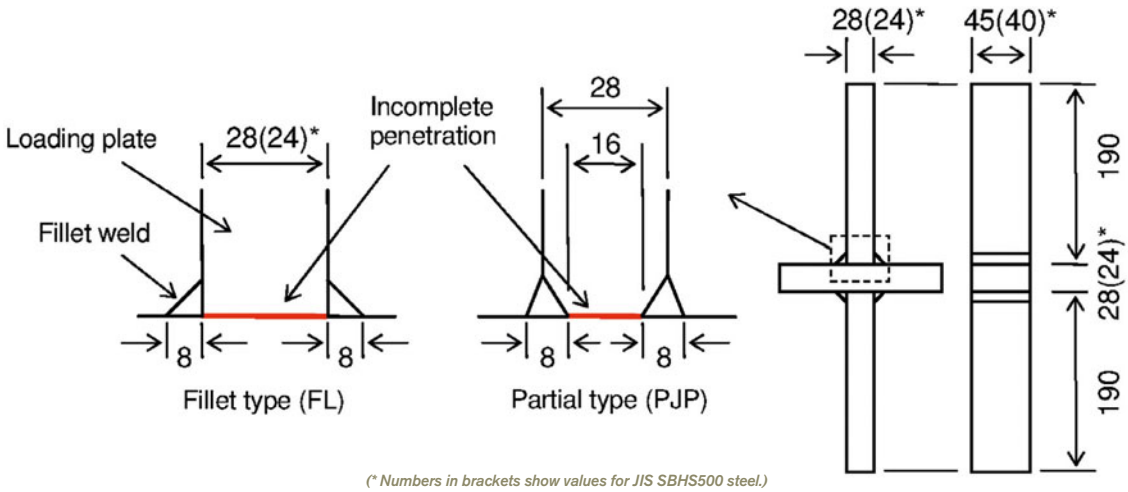

Figure 2 – Specimen dimensions [mm]

joint. Two kinds of under-matching were used for the SBHS500 steel joints.

2.2 Mechanical properties of the weld deposit

Monotonic tensile tests and incremental cyclic loading tests were performed to determine the material properties of the weld deposit in each specimen type. As shown in Figure 3, use was made of round bar-type test specimens which were cut out from the weld deposit and the base metal.

2.2.1 Monotonic tensile loading tests

Monotonic tensile tests were carried out to determine the yield strengths of the weld deposit and the base metal. True strain in the loading direction was calculated from the change in diameter of the throat of the specimen, measured by a displacement transducer. Figure 4 shows the tensile test results. The yield strengths from the tensile tests are compared with those from the welding wire catalogues in Table 2. Also shown are the matching ratios (WD/BM), under-matching joints having a value below 1. As will be seen, the weld deposit over-matched the SM490 steel by around 25 % to 45 %, while they under-matched the SBHS500 steel by around 10 % to 20 %. The specimens were identified according to the welding conditions and the matching ratio, as listed in Table 3.

It will be noted from Table 2 that the measured and catalogue values of weld deposit yield strength differed. This may be because the mechanical properties of the weld deposit can be affected by the cooling speed and mixture of material composition in the deposit. From a practical viewpoint, the results indicate that the strength matching condition for a welded joint cannot be properly estimated from catalogue values of welding wire strength. Thus, tests on actual weld deposits are required for accurate determination of the matching conditions. Regarding the SM490 base metal, it is not known why the measured and inspection certificate sheet yield strengths differed.

2.2.2 Incremental cyclic loading tests

Cyclic stress-strain characteristics of the material, like cyclic hardening or softening behaviour, were confirmed by the incremental cyclic tests. Figure 5 shows examples of the incremental cyclic stress-strain relationships together with the tensile test results. In the SM490 base metal, a cyclic stress-strain curve, defined as the locus of tips of hysteresis loops, locates slightly lower than a tensile curve in the strain region less than 0.005 which indicates cyclic softening behaviour. Similar but small cyclic

Table 2 – Mechanical properties of materials

Material		Catalogue values	Tensile test results	
		Yield strength [MPa]	Yield strength [MPa]	Matching ratio (WD/BM)
SM490 (BM)		451[a]	392	–
Weld deposit (WD)	O45	450	565	1.44
	O25-1	380	498	1.27
	O25-2	380	494	1.26
SBHS500 (BM)		573[a]	554	–
Weld deposit (WD)	U10	480	491	0.89
	U20	380	451	0.81

[a] Yield strength of base metal is based on the inspection certificate sheet.

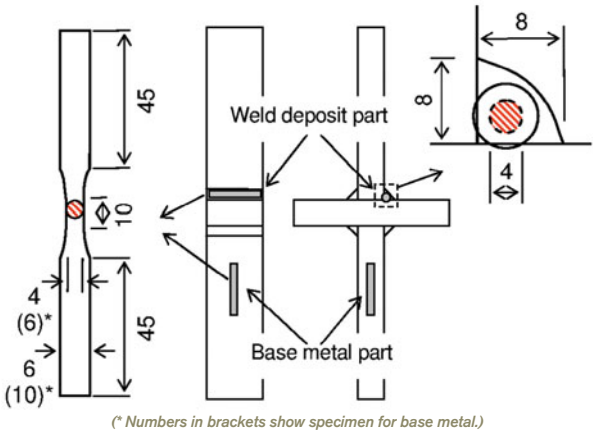

(* Numbers in brackets show specimen for base metal.)

Figure 3 – Round bar-type specimen for material tests [mm]

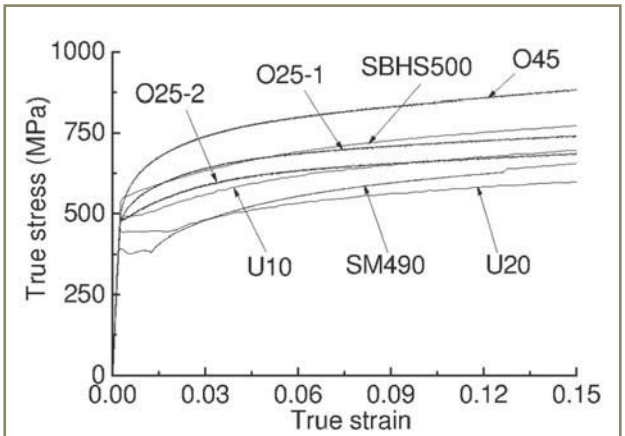

Figure 4 – Tensile test results of materials

Table 3 – Specimen names

Base metal	JIS SM490						JIS SBHS500	
Welding type	Fillet weld (FL)			Partial joint penetration groove weld (PJP)			Fillet weld (FL)	
Welding conditions	1	2	4	1	2	4	1	3
Welding wire	YM-24S	YM-24S	YM-28	YM-24S	YM-24S	YM-28	YM-24S	YM-28S
Width [mm]	45	45	45	40	40	40	40	40
Thickness [mm]	28	28	28	28	28	28	24	24
Name	FL-O25-1	FL-O25-2	FL-O45	PJP-O25-1	PJP-O25-2	PJP-O45	FL-U20	FL-U10

softening behaviour can be observed in the base metal of SBHS500, the weld deposit of O25-2, U10 and U20. However, after a strain exceeding about 0.005, their cyclic stress-strain curves are higher than the tensile curves, meaning cyclic hardening behaviour. The weld deposit of O45 and O25-1 displayed cyclic hardening throughout the plastic strain region. Therefore, all materials in the specimens represent cyclic hardening behaviour in most of the plastic strain region.

2.3 Measurements of incomplete penetration

In order to locate the weld deposit, base metal and heat-affected zones, macro etch tests were carried out. The etched surfaces of fillet and partial type specimens are shown in Figure 6.

Table 4 shows the average values of the weld size (H_1, H_2), root size (2a), fusion size (p) and throat thickness

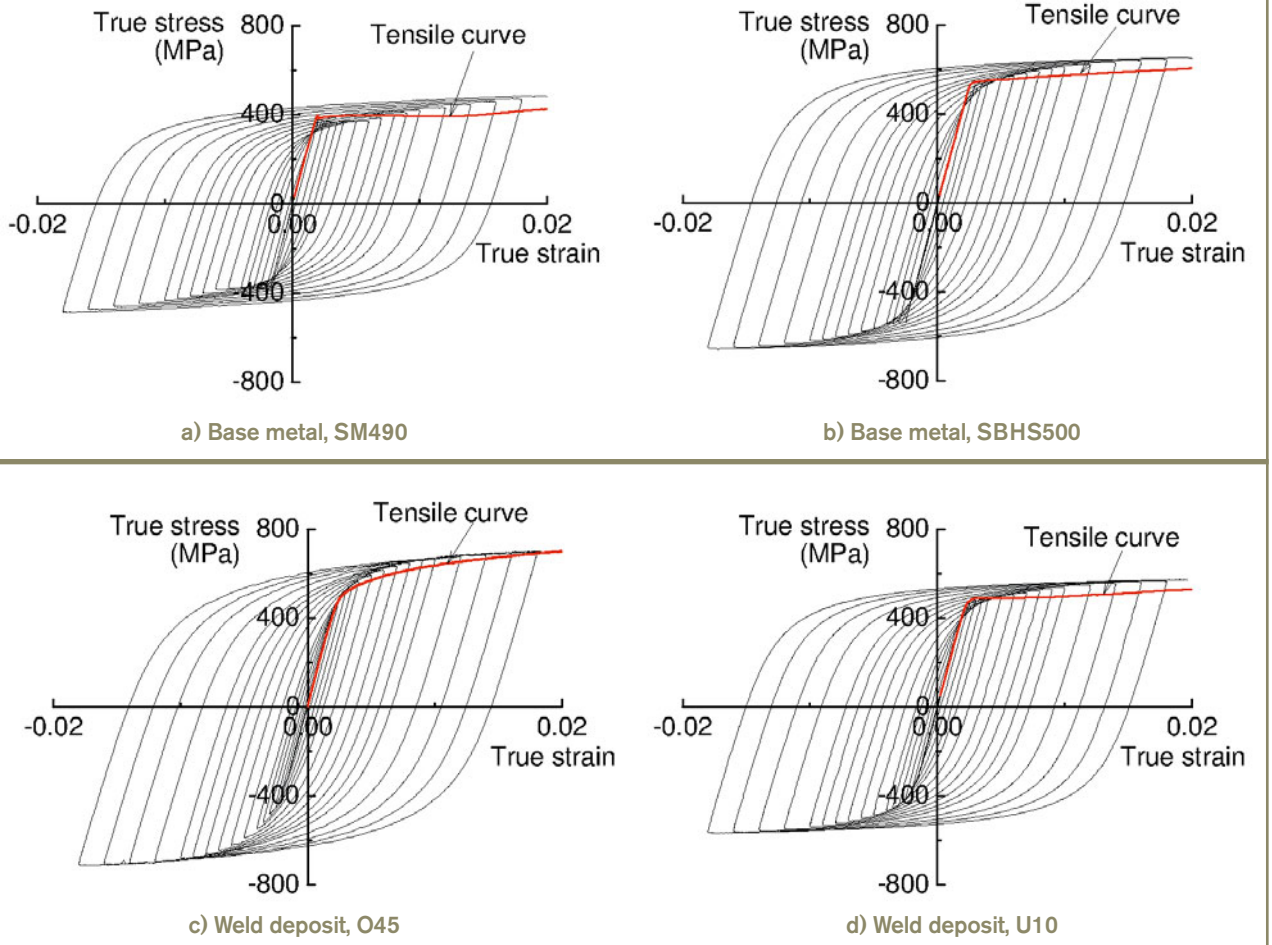

a) Base metal, SM490

b) Base metal, SBHS500

c) Weld deposit, O45

d) Weld deposit, U10

Figure 5 – Cyclic hardening behaviour of the base metal and weld deposit

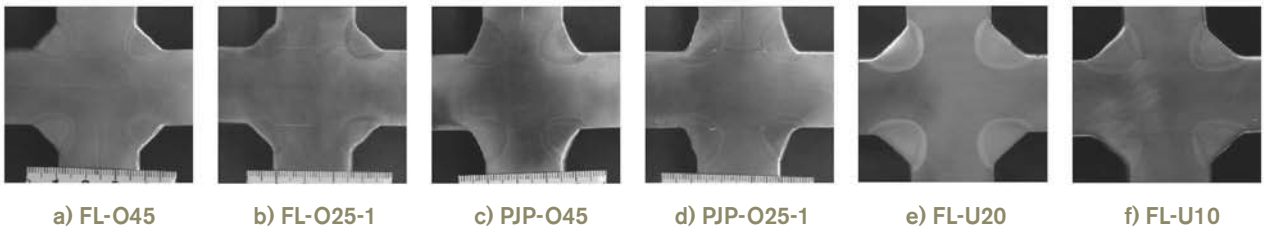

a) FL-O45 b) FL-O25-1 c) PJP-O45 d) PJP-O25-1 e) FL-U20 f) FL-U10

(Loading direction: up-and-down.)

Figure 6 – Macro etch test results

Table 4 – Average values in measurements of the welded portion

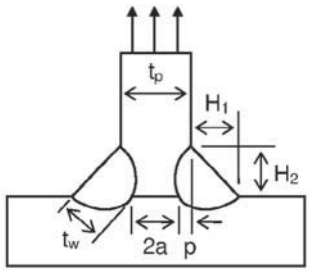

Specimen	t_p [mm]	H_1 [mm]	H_2 [mm]	2a [mm]	p [mm]	t_w [mm]	H_1/t_p	$2a/t_p$
FL-O45	28	8.84	8.86	23.00	2.50	8.09	0.32	0.82
FL-O25-1	28	8.99	8.80	24.12	1.94	7.74	0.32	0.86
FL-O25-2	28	9.56	9.07	24.54	1.73	7.96	0.34	0.88
PJP-O45	28	6.14	11.28	17.60	5.20	9.37	0.22	0.63
PJP-O25-1	28	6.11	11.31	17.34	5.33	9.39	0.22	0.62
PJP-O25-2	28	5.13	10.86	16.96	5.52	9.59	0.18	0.61
FL-U10	24	9.09	9.17	17.52	2.77	8.56	0.38	0.73
FL-U20	24	9.18	9.32	18.69	2.31	8.24	0.38	0.78

(t_w) measured from the photos. Referring to earlier research [5, 7], parameters of $2a/t_p$ and H_1/t_p in the specimen, where t_p is the thickness of the loading plate, are consistent with conditions which ensure the failure occurs from the weld root, rather than the weld toe, in the high-cycle fatigue region. The ratios $2a/t_p$ and H_1/t_p in the specimens ranged from 0.61 to 0.88 and 0.18 to 0.38, respectively.

3 Experimental procedures

In this study, tensile tests, low-cycle fatigue tests and high-cycle fatigue tests were conducted.

3.1 Tensile tests

The monotonic tensile tests were performed on a 2 000 kN-capacity testing machine. For measurements of deformation around the weld portion, 50 mm gauge length PI displacement transducers were mounted on both sides of the loaded plate over the weld roots, as shown in Figure 7. The tensile results are represented in Figure 8 in terms of stress in the loaded plate versus the average strain calculated from the displacements of two PI gauges. The stress in the loaded plate was generally less than the yield strength of the base metal. Relatively low elongation can be observed in specimen FL-O25-2 compared to others.

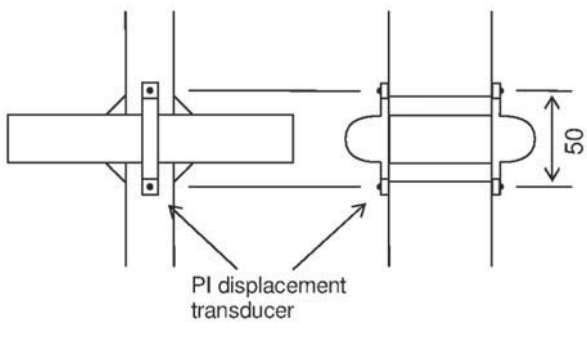

(Dimensions in mm.)

Figure 7 – Locations of PI displacement transducers

3.2 Low-cycle fatigue tests

The fatigue testing machine was an electric hydraulic servo system with a dynamic and a static loading capacity of 300 kN and 450 kN. Low-cycle fatigue tests were controlled by the value of the displacement transducer

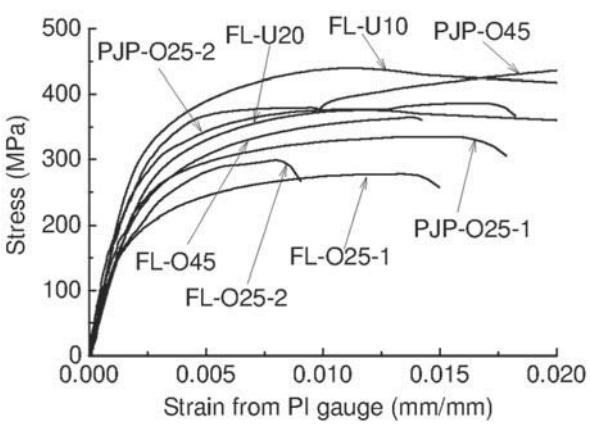

Figure 8 – Tensile test results for welded joint specimens

attached to the same location as the tensile test, giving the constant displacement range of 0.18 mm, 0.23 mm, 0.28 mm and 0.33 mm. The ratio of the minimum and the maximum displacement ranged from 0.06 to 0.1. Cyclic load with a very low displacement rate of approximately from 0.0017 mm/s to 0.0082 mm/s was applied to the specimen.

Test conditions are summarized in Table 5. The maximum and the minimum stress in loading plates were calculated from the maximum and the minimum load at the first cycle. It can be found that the stress in the loaded plate was lower than the yield strength of the base metal, meaning that the loaded plate showed elastic behaviour during the test.

For the specimen with 0.28 mm and 0.33 mm displacement range, the specimen was loaded monotonically to break completely after a fatigue crack had propagated through one weld. For the displacement range of 0.18 mm and 0.23 mm, the test was stopped after the load dropped by 30 % from the maximum load at the initial loop, to measure the crack length into the weld deposit at 30 % load drop.

3.3 High-cycle fatigue tests

High-cycle fatigue tests were conducted under load-control conditions. The stress range, calculated by dividing the load range by the measured weld throat area, was around 140 MPa to 180 MPa. The stress ratio was about 0.05. A sinusoidal waveform with a frequency of 10 Hz was used. Two-step block loading tests (beach mark tests) were also performed. The tests were continued until specimen rupture.

4 Experimental results

4.1 Crack initiation and propagation

Figure 9 shows the various stages of crack propagation behaviour as observed on the side surface of a specimen during the test, and crack lengths measured from the photographs are summarized in Figure 10. After the first cycle, large plastic deformation was observed around the root tip and a small crack from the tip was first detected after only 10 cycles. The crack gradually grew with the loading repetition.

Figure 11 indicates the fracture surfaces of ruptured specimens in which the weld root is located in the upper side. In all specimens, a crack initiated at the weld root around the mid-width of the specimen and propagated through the weld throat. The results of beach mark tests are shown in Figure 12. From differences between the load block applied and the number of beach marks on the fracture surface, the number of cycles to crack initiation can be identified. It is noticed that the ratio of the crack initiation period (N_c) to the failure life (N_f) is almost

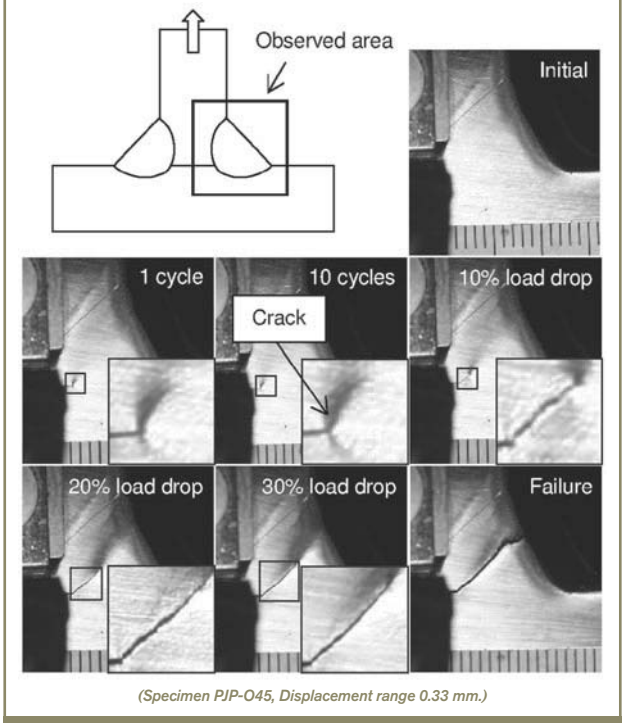

(Specimen PJP-O45, Displacement range 0.33 mm.)

Figure 9 – Crack propagation at side of low-cycle fatigue test

Table 5 – Low-cycle fatigue test conditions

Specimens	Displacement range [mm]	Stress at loading plate [MPa] (Displacement range = 0.33 mm)	
		Maximum	Minimum
FL-O45	0.18, 0.23, 0.33	333.4	-176.4
FL-O25-1	0.18, 0.23, 0.33	262.4	-157.5
FL-O25-2	0.18, 0.23, 0.33	284.7	-173.6
PJP-O45	0.18, 0.23, 0.33	360.2	-274.4
PJP-O25-1	0.18, 0.23, 0.33	310.2	-232.0
PJP-O25-2	0.18, 0.23, 0.33	364.9	-233.5
FL-U10	0.18, 0.23, 0.28, 0.33	419.0	-271.6
FL-U20	0.18, 0.23, 0.28, 0.33	347.3	-240.6

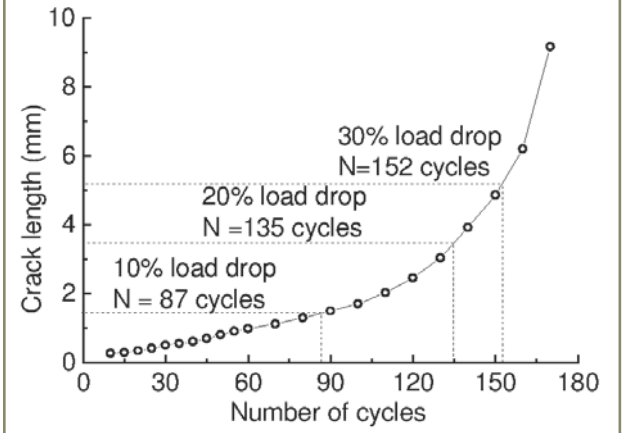

Figure 10 – Crack length and number of cycles

zero, $N_c/N_f = 0.077$ for FL-O45 and $N_c/N_f = 0.063$ for FL-U10, in the high-cycle fatigue region. The results in Figures 9-12 indicate that the fatigue crack originates around the mid-width of the specimen in the early stages of the life. Thus, the crack initiation period can be considered to be extremely small ($N_c \approx 0$) for both low- and high-cycle fatigue.

Previous research has indicated that the relationship between crack initiation period and total failure life in plain material can be dominated by the degree of strain concentration at the crack initiation point. In other words, the ratio of the crack initiation period to the failure life decreases with increasing strain concentration factor [16].

In the load-carrying cruciform joint, an extremely high strain concentration occurs at the tip of the weld root, which explains why the crack initiation period is small in this type of specimen. Consequently, it can be mentioned that crack propagation dominates its fatigue life.

4.2 Failure path

Figure 13 shows the side surfaces of the ruptured specimen, where grey-coloured zones represent the location of the weld deposit and red circles represent weld beads which were first broken by the crack propagating. As for the crack propagation pattern, the tensile and the low-cycle fatigue specimen are similar. The crack tends to propagate in a straight line at a low angle to the loaded plate. On the other hand, the crack runs perpendicular to the loading direction then begins to propagate obliquely in the high-cycle fatigue test. Regarding the effect of the strength matching, different crack patterns can be observed in the low-cycle fatigue specimen. Cracking paths in the specimens with lower matching ratio tend to become closer to the loaded plate. However, in the high-cycle fatigue specimen, the crack propagates in almost the same pattern, despite the difference in the matching condition.

4.3 Load-displacement hysteresis loops

Figure 14 shows an example of the load-displacement relationship in the low-cycle fatigue test in which the displacement range from PI gauge was 0.33 mm. Figure 15

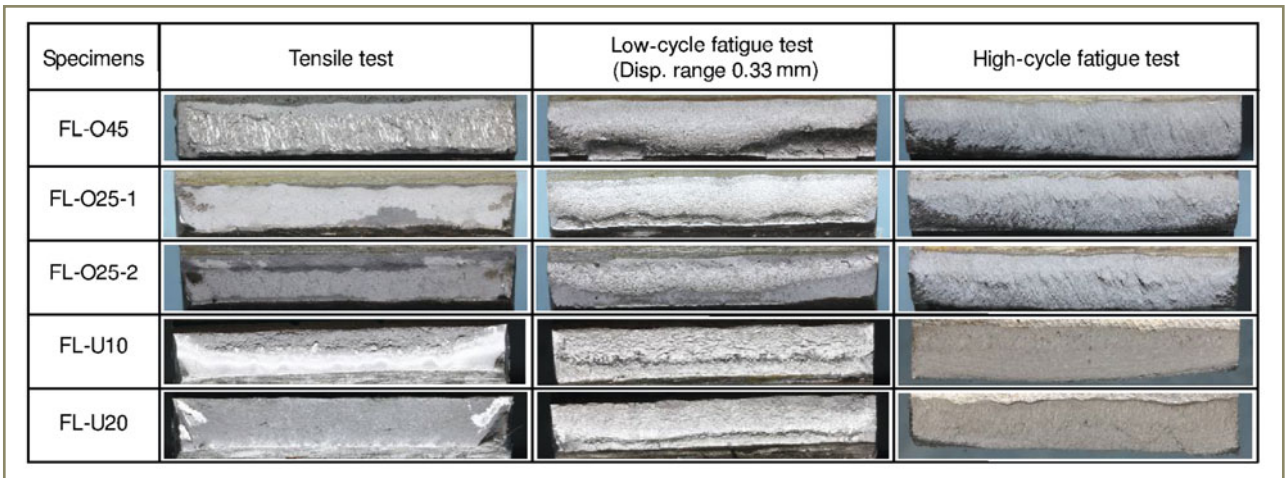

Figure 11 – Fracture surfaces

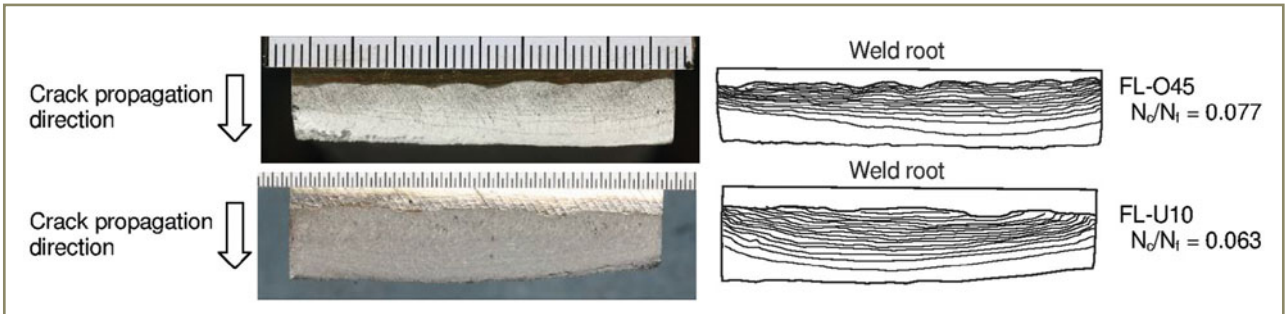

Figure 12 – Beach marks of high-cycle fatigue specimens

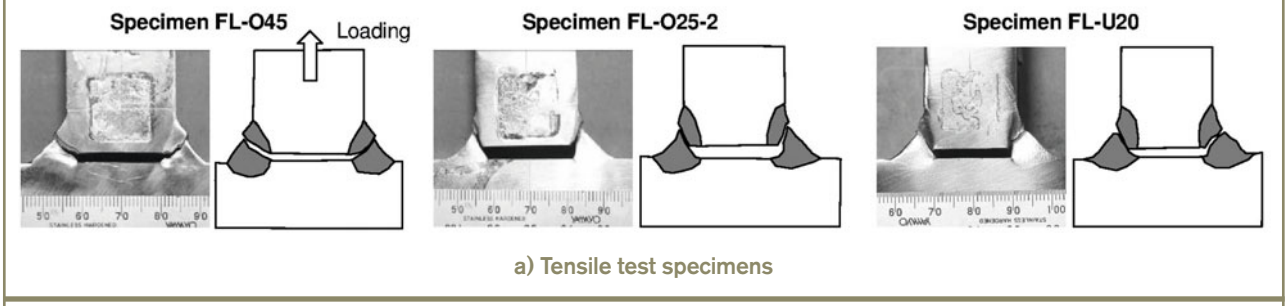

a) Tensile test specimens

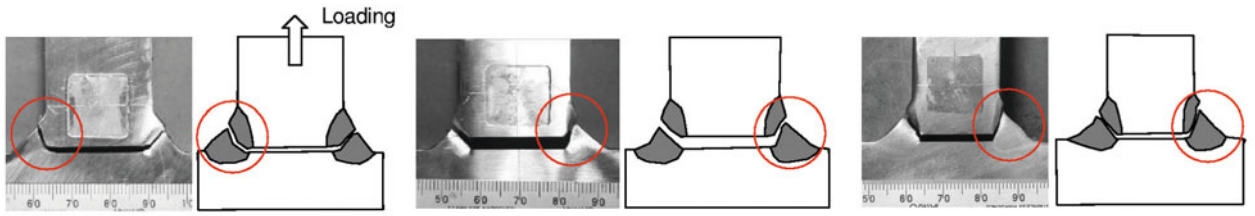

b) Low-cycle fatigue test specimens (Disp. range 0.33 mm)

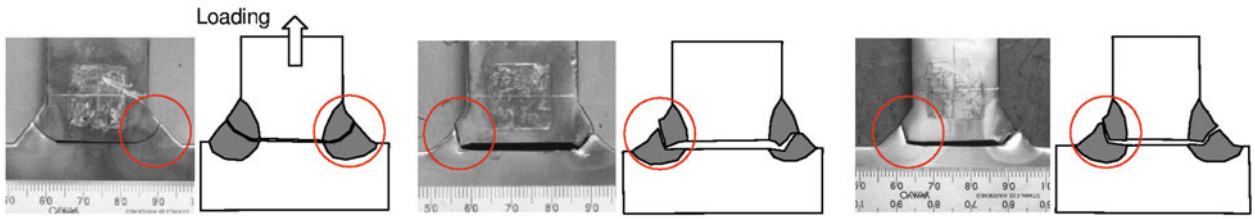

c) High-cycle fatigue test specimens

(Circles indicated failure from fatigue cracking, loading direction is up-down.)

Figure 13 – Crack propagation paths

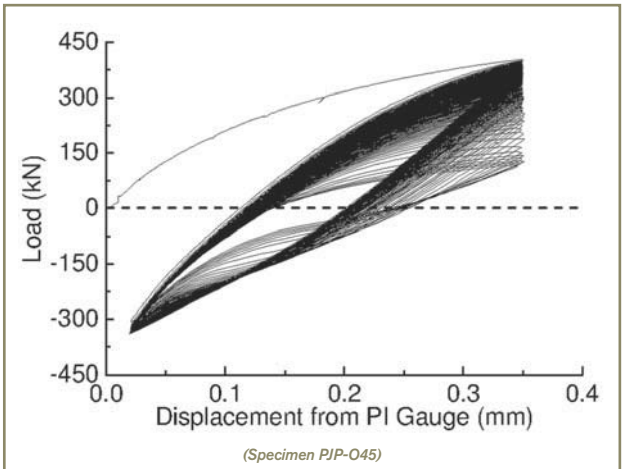

(Specimen PJP-O45)

Figure 14 – Load-displacement relationship in the low-cycle fatigue test

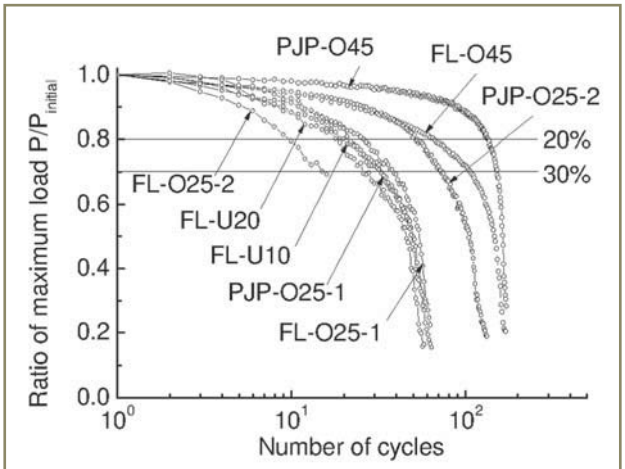

Figure 15 – Relationship between the maximum load at each loop and number of cycles

shows the relationship between the change of maximum load and number of cycles when the displacement range was 0.33 mm. The ordinate represents the ratio of the maximum load of each cycle to that at the initial cycle. The maximum load is decreasing with the load repetition, although the weld deposit shows cyclic hardening behaviour, as shown in Figure 5. This load decrease is caused by the presence of a fatigue crack in the early cycles and its growth with cyclic loading.

4.4 Definition of fatigue life in low-cycle fatigue

As stated above, the failure life of the load-carrying cruciform joints is governed by crack propagation, and the load continues to decrease with loading repetitions. Figure 15 reveals that the maximum load gradually decreases until around 20 % load drop and begins to decline rapidly after 30 % load drop. In this study, therefore, the fatigue life for

the low-cycle fatigue tests was defined as the number of cycles to 20 % load drop.

4.5 Fatigue life

4.5.1 Low-cycle fatigue tests

Figure 16 shows the low-cycle fatigue test results for SM490 and SBHS500, respectively. As defined above, the fatigue life is the number of cycles when the maximum load drops by 20 %. The results were represented by the stress range on the weld throat section. It can be seen that the strength matching has a significant influence on the low-cycle fatigue strength, as the specimen with a lower matching ratio shows obviously low fatigue strength.

As to the effect of the incomplete penetration size, no noticeable difference between FL and PJP type specimens can be observed in Figure 16 a), although parameters of $2a/t_p$ and H_1/t_p in the specimen, where $2a$, t_p and H_1 are given in Table 4, are different in each type. This may be because the ratio of a/W ($W = H_1 + t_p/2$), which is one of the parameters to calculate the stress intensity factor for the load-carrying cruciform joint [5], is relatively close in all specimens, 0.51 for FL type and 0.44 for PJP type. Therefore, it is possible that the parameter of a/W is a factor governing the low-cycle fatigue strength of load-carrying cruciform joints.

4.5.2 High-cycle fatigue tests

Figure 17 shows the high-cycle fatigue test results plotted in terms of the stress range on the weld throat. Design S-N curves recommended in JSSC specifications [17] are also shown. The results indicate that the fatigue strengths for both the over- and the under-matched joints are almost the same. Therefore, it is obvious that the effect of the strength mismatch is negligible in the high-cycle fatigue region.

4.6 Detailed observation

4.6.1 Crack length at 30 % load drop

The low-cycle fatigue tests applying a 0.23 mm displacement range were stopped at 30 % load drop. The welded part of the specimen was sliced at the mid-width and examined under a microscope. An example is shown in Figure 18. The measured crack length is listed in Table 6. It was found that the crack length at 30 % load drop was approximately 2-5 mm, close to half of the weld throat.

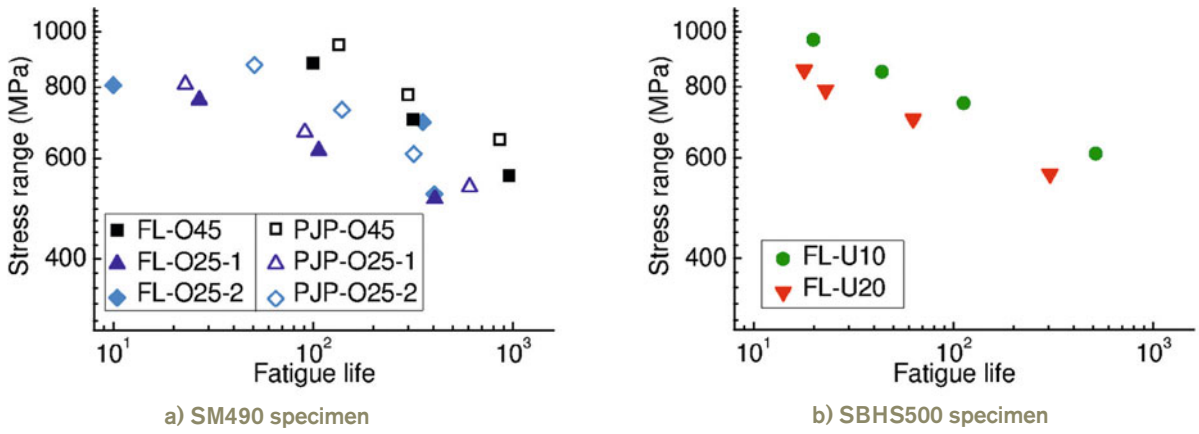

a) SM490 specimen b) SBHS500 specimen

Figure 16 – Results of low-cycle fatigue tests

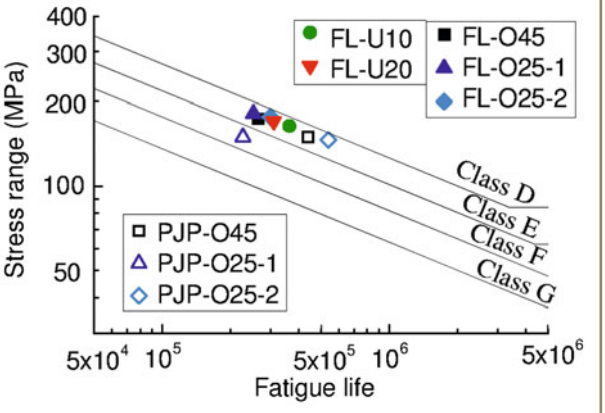

Figure 17 – Results of high-cycle fatigue tests

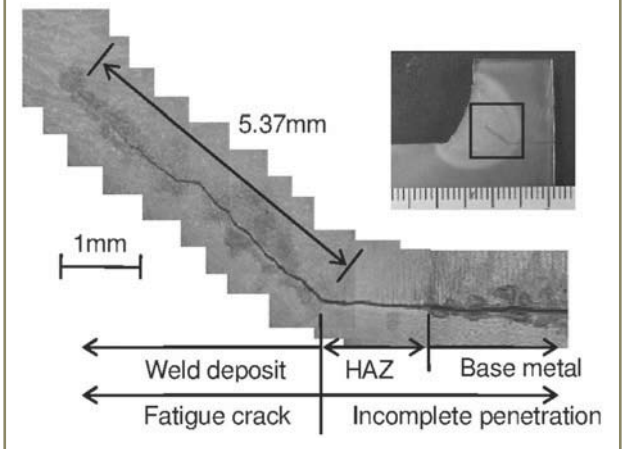

Figure 18 – Crack length at 30 % load drop (PJP-O45)

4.6.2 Fractography

Figure 19 shows fractographs taken from the tensile, the low-cycle fatigue and the high-cycle fatigue specimens at the location close to the weld root around the mid-width. The weld root is located at the upper side of the picture, and the crack penetrates downward. The fractograph corresponding to the low-cycle fatigue test shows evidence of dimples that have been compressed by the cyclic loading [18]. Dimple patterns can be also observed in the tensile fracture surface. As a result of the fractograph, it can be concluded that ductile crack propagation is predominant in the low-cycle fatigue regime.

5 Strain analyses

It has been confirmed that the crack initiation period in the low-cycle fatigue regime correlates strongly with the plastic strain range at the crack initiation site, the well-known Manson-Coffin law [19, 20]. The relationship is applicable to a notched specimen [16, 21-23]. Thus, a fatigue crack will initiate in almost the same number of cycles regardless of the notch geometry for a given local strain at a notch tip. This strain-based concept has served as a foundation for low-cycle fatigue design in the ASME Boiler and Pressure Vessels Code, Sec. III. In this study, therefore, finite element analyses were performed to determine the local strain fields around the weld root tip, in order to establish the link between the fatigue life of the specimen and the local strain range at the tip. In the analyses, the concept of the fictitious notch [24] was adopted in order to avoid the effect of stress singularity at the root tip.

5.1 Analysis Methods

5.1.1 FE model

Figure 20 shows an example of an FE model for a load-carrying cruciform welded joint. 2D solid elements under plane-strain conditions were performed with ABAQUS code. By taking advantage of symmetry, a one-quarter symmetry model was created.

The analysis models were created individually according to the measurements of the welded parts listed in Table 4. The concept of the fictitious notch with radius of 1.0 mm [24] was applied at the weld root tip in order to avoid the effect of stress singularity, as illustrated in Figure 20. Otherwise, for quantitative comparison among all models, the vicinity of the root tip was meshed in the same configuration. The minimum element size along the notch was 0.05 mm, which satisfies the IIW recommendation [24].

According to the etching surface of each specimen in Figure 6, the base metal region (BM), the weld deposit region (WD) and the heat-affected zone (HAZ) were identified. Each region was separately created in analysis model, as shown in Figure 20. Different stress-strain relationships shown in Figure 21 were assigned to each zone, which were obtained from the identification results as discussed below in detail.

When the circumference of the fictitious notch was located at the crack tip, as stated in the IIW recommendation [24], the boundary of the weld deposit and the HAZ overlaid the circumference of the notch, which made it difficult to provide uniform element geometry along the

Table 6 – Summary of crack length at 30 % load drop

Specimen	FL-O45	FL-O25-1	FL-U10	FL-U20	PJP-O45	PJP-O25-1	PJP-O25-2
Crack length [mm]	1.93	2.55	2.61	2.70	5.37	3.20	4.02

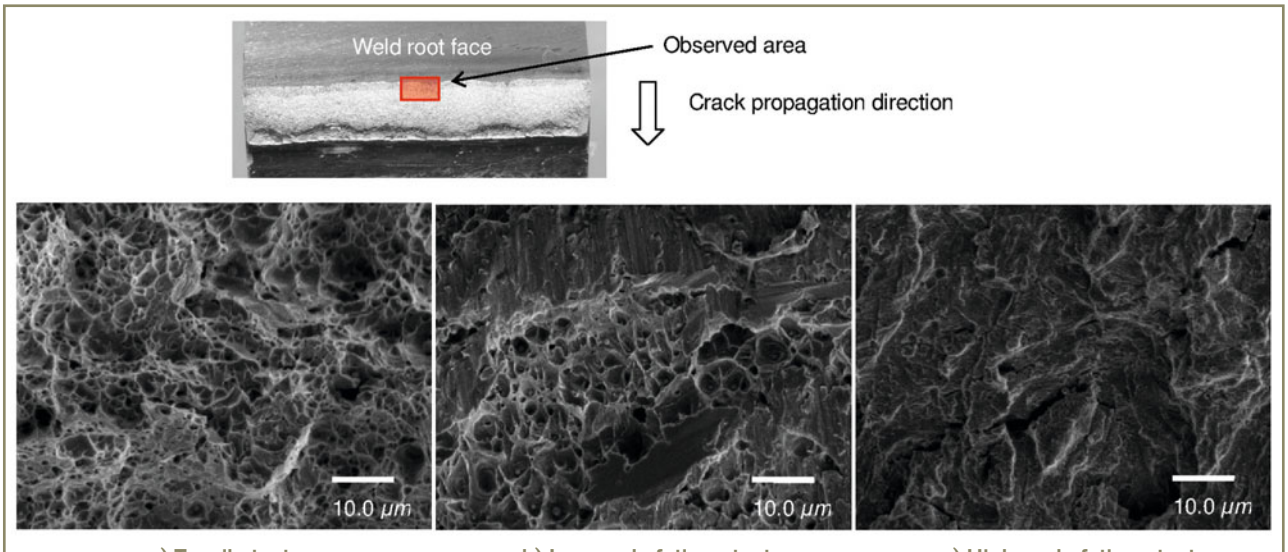

a) Tensile test | b) Low-cycle fatigue test (Displacement range. 0.33 mm) | c) High-cycle fatigue test

Figure 19 – Fractography of specimen FL-O25-1 (×1000)

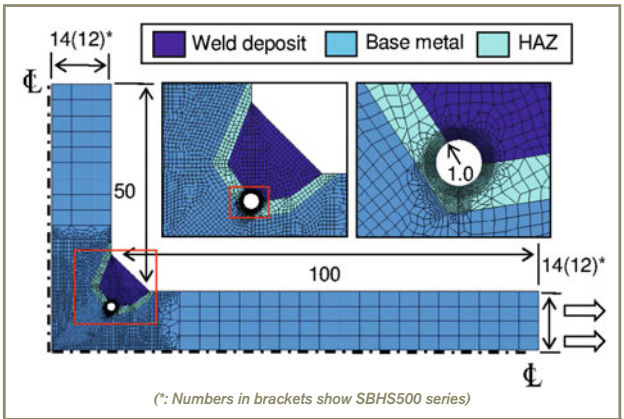

Figure 20 – Global view of finite element model [mm]

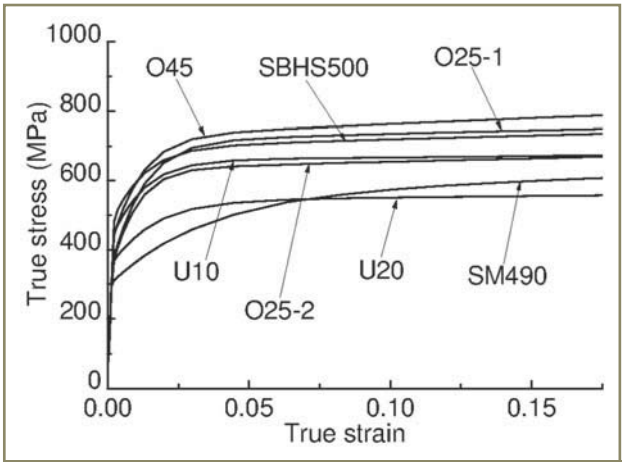

Figure 21 – Stress-strain relationship for analysis

notch. Thus, it was assumed that the boundary between the weld deposit and the HAZ passed the centre of the notch, as shown in Figure 20.

The analysis conditions were set to be the same as in the experiments, applying tensile and compressive loads through the loading plate with displacement control. In the analysis, crack initiation and propagation was not considered.

5.1.2 Material parameters

A yield function given in the following equations was employed for each material which consists of isotropic and kinematic hardening rules [25].

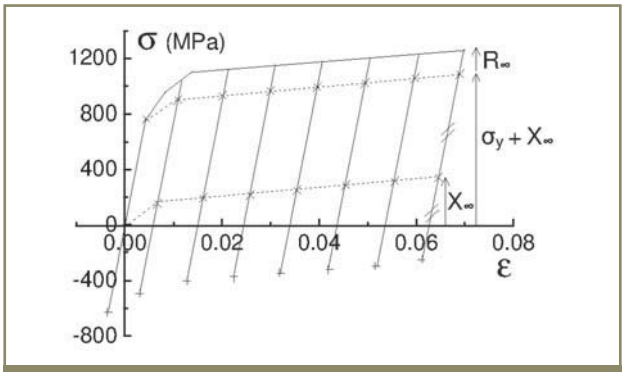

Figure 22 – Definition of hardening parameters

$$f = \sigma - X - R - \sigma_y \quad (1a)$$

$$R = R_\infty(1 - \exp(-b \cdot \varepsilon_p)) \quad (1b)$$

$$X = X_\infty(1 - \exp(-\gamma \cdot \varepsilon_p)) \quad (1c)$$

where

R is the isotropic hardening,

X is the back stress,

σ_y, R_∞, b, X_∞, γ are material parameters given in Figure 22,

ε_p is the plastic strain.

Concerning cyclic hardening behaviour, isotropic and kinematic parameters were identified for each material based on tensile curves with repeated unloadings until the compressive yield strength was reached, as presented in Figure 22. The material tests, as illustrated in the figure, were performed using the round bar-type specimens shown in Figure 3. The results of identified isotropic and kinematic parameters are listed in Table 7. In order to confirm the precision of the hardening parameters, the analysis with the hardening parameters in Table 7 was carried out under the same conditions as the material tests. There was relatively good agreement between the analysis results and the material test results, as shown in Figure 23.

Table 7 – Hardening parameters

Material		σ_y [MPa]	Isotropic		Kinematic	
			R_∞ [MPa]	b	X_∞ [MPa]	γ
SM490 (BM)		304	143	4	233	33
Weld deposit (WD)	O45	435	387	1	292	106
	O25-1	367	95	3	284	163
	O25-2	351	223	1	283	124
SBHS500 (BM)		493	143	2	201	97
Weld deposit (WD)	U10	446	96	1	212	96
	U20	362	98	1	180	69

For the yield function of the HAZ, it was assumed to have a 20 % higher yield strength than that of the base metal, and the same isotropic and kinematic hardening parameters as the base metal. Young's modulus was assumed to be 200 GPa, and Poisson's ratio was 0.3 and 0.5 before and after yielding, respectively.

5.2 Analysis results

5.2.1 Load-displacement hysteresis loops

The global behaviour of each FE model was compared with the experimental result. As Figure 24 shows, there was good agreement indicating that the FE modelling was a relatively accurate representation of the experiment.

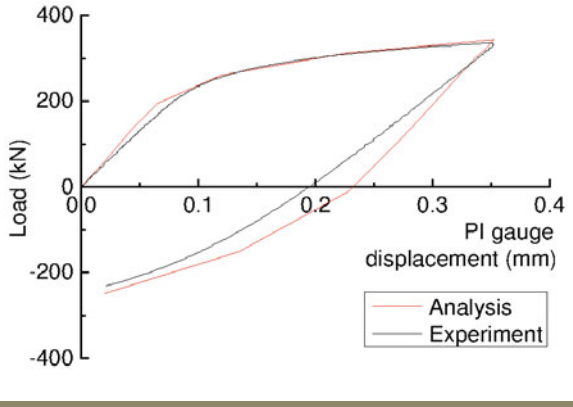

Figure 24 – Comparison of load-displacement relationship

5.2.2 Strain around the weld root tip

Local strain distributions around the root tip are compared in Figure 25. The contours represent the distributions of equivalent plastic strain around the root tip when applying the maximum tensile displacement. In the figure, the strain scale shown in the figure applied to all four of the contour plots given. It is obvious that equivalent plastic strain concentration around the tip in FL-U20 is higher than for the others. Consequently, relatively high strains are induced to the weld deposit in under-matching joints.

5.2.3 Fatigue assessment by using local strain

Figure 26 shows the relation between the local strain range at the weld root and the fatigue life. The local strain range was obtained in elements along the fictitious notch which had the maximum value of the equivalent

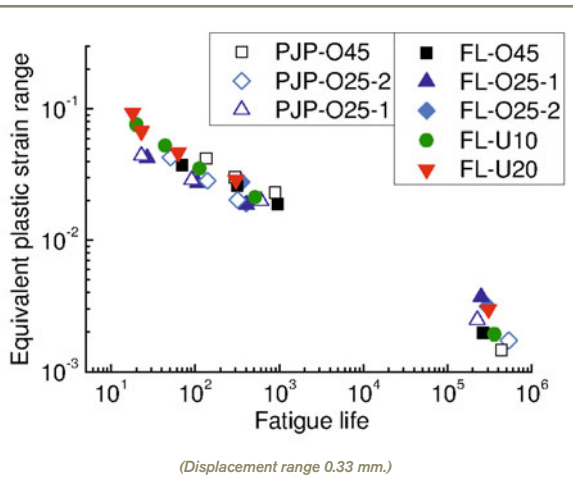

Figure 26 – Relationship between equivalent plastic strain range and matching ratio

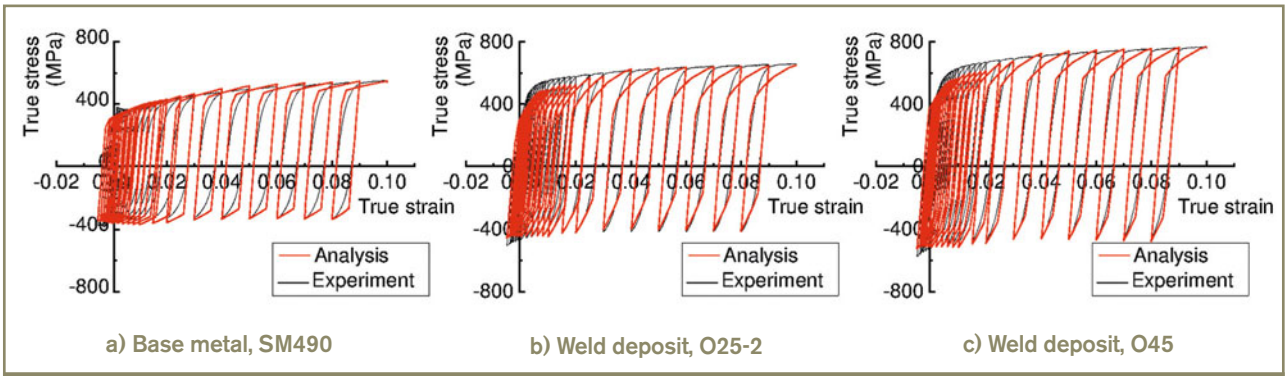

a) Base metal, SM490 b) Weld deposit, O25-2 c) Weld deposit, O45

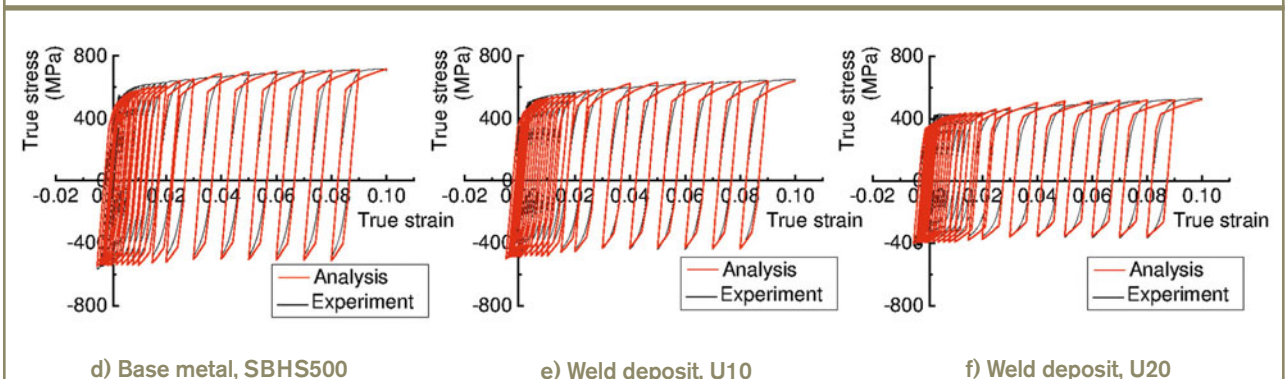

d) Base metal, SBHS500 e) Weld deposit, U10 f) Weld deposit, U20

Figure 23 – Comparisons of results from experiments and analyses using hardening parameters

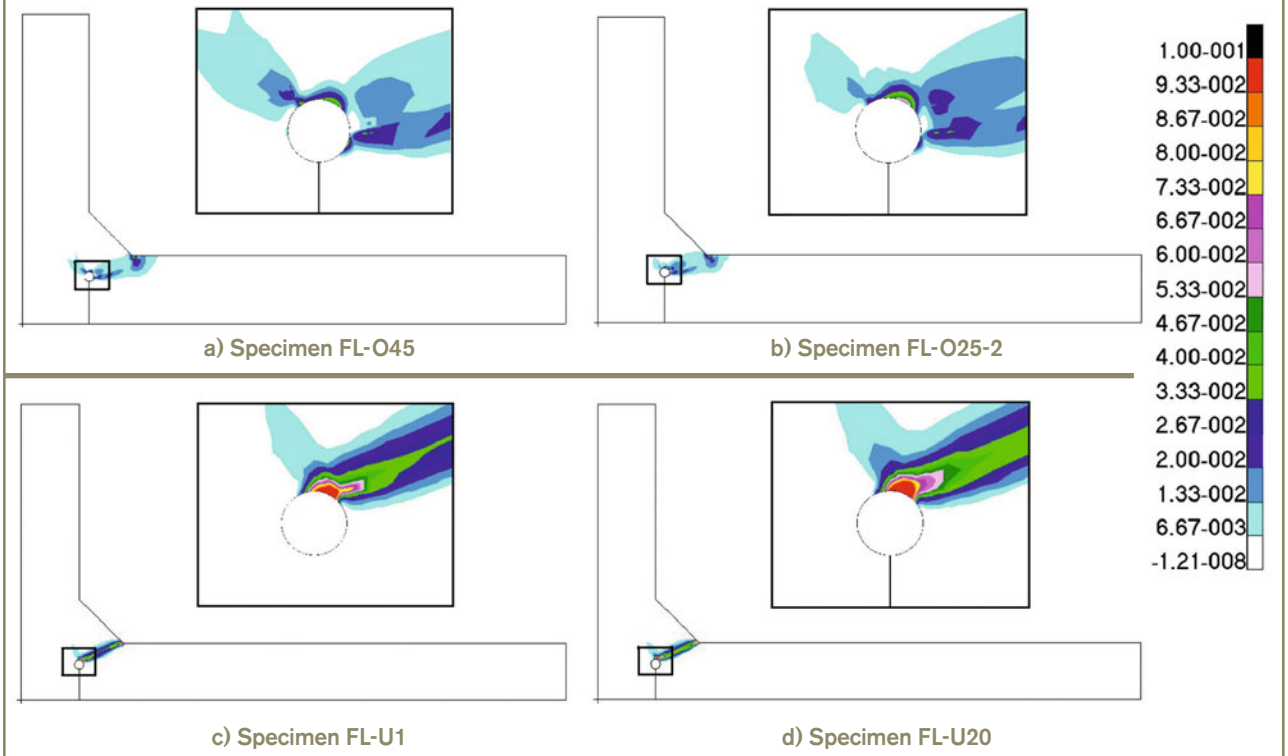

Figure 25 – Distribution of equivalent plastic strain at PI gauge displacement of 0.35 mm

plastic strain range. It will be noted that by characterizing the fatigue strength of the specimen using local strain, a unique S-N curve can be established from the low- to high-cycle fatigue regime. As a result, the local strain approach can be used to assess the fatigue strength of load-carrying cruciform joints in both the low- and high-cycle fatigue regions.

6 Conclusions

In this study, the low- and high-cycle fatigue strengths of load-carrying cruciform welded joints containing various incomplete penetration sizes and strength mismatch were investigated. The following summarizes the findings:

1. The value of yield strength from the catalogue of welding wires cannot be relied upon to estimate matching conditions in actual welded joints. Thus, material tests of the weld deposit are required to reveal the true strength matching condition.
2. For both the low- and high-cycle fatigue region, the crack initiation point was located at the weld root around the mid-width of the specimen. Then, the crack propagated through the weld throat.
3. For low-cycle fatigue conditions, the fatigue crack initiates very early on in the life ($N_c \approx 0$ cycles). Thus, the fatigue life is dominated by crack propagation.
4. Strength matching between the weld deposit and the base metal has significant influence on the low-cycle fatigue strength, but is negligible in the high-cycle fatigue region.
5. The low-cycle fatigue performance is influenced because weld under-matching causes higher plastic strains in the weld which concentrate at the weld root and thus reduce the fatigue strength of the joint.
6. Local strain approach can be used to assess the fatigue strength of the cruciform joint specimen in both the low- and high-cycle fatigue regimes.

Acknowledgements

The authors gratefully acknowledge the support of the Grant-in-Aid for Scientific Research (S) (18106010) in Japan and the Research Fund for Young Researchers under the Center for Urban Earthquake Engineering (CUEE) in Tokyo Institute of Technology. The authors would like to express sincere gratitude to Mr. Takebuchi at TTES, Inc. and Mr. Yoneyama at KAWADA Industries, Inc. in Japan for fabricating the specimens.

References

[1] Miki C. and Hirabayashi Y.: Fatigue damage cases due to inappropriate fabrication in steel bridge structures, Doboku Gakkai Ronbunshuu A, JSCE, 2007, vol. 63, no. 3, pp. 518-532 (in Japanese).

[2] Miki C.: Retrofitting engineering for fatigue damaged steel structures, IIW Doc. XIII-2284r1-09, 2010.

[3] Miki C.: Fatigue and fracture issues of welds in civil structures, Science and Technology of Welding and Joining, 2000, vol. 5, no. 6, pp. 347-355.

[4] Gurney T.R.: Fatigue of welded structure, 2nd edition, Syndics of the Cambridge University Press, 1979.

[5] Frank K.H. and Fisher J.W.: Fatigue strength of fillet welded cruciform joints, Journal of Structural Division, ASCE, 1979, vol. 105, no. ST9, pp. 1727-1740.

[6] Maddox S.J.: Fatigue strength of welded structures, 2nd edition, Abington Publishing, 1991.

[7] Miki C., Tateishi K., Fan H. and Tanaka M.: Fatigue strengths of fillet-welded joints containing root discontinuities, International Journal of Fatigue, 1993, vol. 15, no. 2, pp. 133-140.

[8] Kainuma S. and Mori T.: A fatigue strength evaluation method for load-carrying fillet welded cruciform joints, International Journal of Fatigue, 2006, vol. 28, no. 8, pp. 864-872.

[9] Kainuma S. and Mori T.: A study on fatigue crack initiation point of load-carrying fillet welded cruciform joints, International Journal of Fatigue, 2008, vol. 30, no. 9, pp. 1669-1677.

[10] Ishii Y. and Iida K.: Low and intermediate cycle fatigue strength of butt welds containing weld defects, Journal of JSNDI, 1969, vol. 18, no. 10, pp. 443-474.

[11] Kyuba H., Fahimuddin F., Machida F. and Miki C.: Low cycle fatigue bahaviour of butt-welded joints with embedded defects, IIW Doc. XIII-1829-00, 2000.

[12] Kayamori Y., Seto A., Masuda T., Machida S. and Miki C.: Influence of weld defects on very low cycle fatigue properties of welded joints, ASME International, PVP427, 2001, pp. 1-8.

[13] Satoh K. and Seo K.: Mechanical behaviour and strength of front fillet welded joint, Journal of JWS, 1972, vol. 41, no. 10, pp. 1182-1196 (in Japanese).

[14] Satoh K., Toyota M. and Fujii E.: Tensile behaviors and strength of soft welded joints, Journal of SNAJ, 1972, no. 132, pp. 381-393 (in Japanese).

[15] Kyuba H., Fukuda Y. and Miki C.: Cyclic loading capacity of butt welded joints with various matching conditions, IIW Doc. XIII-1886-01, 2001.

[16] Miki C., Nishimura T., Tanabe H. and Nishikawa K.: Study on estimation of fatigue strengths of notched steel members, Proceedings of JSCE, 1981, no. 316, pp. 153-168.

[17] Japanese Society of Steel Construction, Fatigue design recommendations for steel structures, Gihodo Shuppan, 1993.

[18] Kuwamura H.: Transition between fatigue and ductile fracture in steel, Journal of Structural Engineering, ASCE, 1997, vol. 123, pp. 864-870.

[19] Manson S.S.: Behavior of materials under conditions of thermal stress, NACA Technical Note, 2933, 1953.

[20] Coffin L.F. Jr.: A study of the effects of cyclic thermal stresses on a ductile metal, Transactions of the ASME, 1954, vol. 76, pp. 931-950.

[21] Manson S.S. and Hirschberg M.H.: Crack initiation and propagation in notched fatigue specimens, NASA Technical Memorandum, X-52126, 1965.

[22] Iida K.: Notch effects in low cycle fatigue of steels, Selected papers from the Journal of SNAJ, 1973, vol. 11, pp. 117-134.

[23] Murakami Y. and Kusumoto S.: Notch effect in low-cycle fatigue, 1st report low-cycle fatigue strength of 0.48% carbon steel under constant load amplitude, Bulletin of JSME, 1973, vol. 16, no. 101, pp. 1637-1647.

[24] Fricke W.: IIW Recommendation for the fatigue assessment by notch stress analysis for welded structures, Doc. IIW-2006 (XIII-2240-08/XV-1289-08), 2008.

[25] Lemaitre J. and Desmorat R.: Engineering damage mechanics, Springer, 2005.

About the authors

Mr Takeshi HANJI (hanji@civil.nagoya-u.ac.jp), formerly Postdoctoral Research Assistant in the Department of Civil Engineering, Tokyo Institute of Technology is now Associate Professor in the Department of Civil Engineering, Nagoya University, Nagoya (Japan). Prof. Chitoshi MIKI (miki@cv.titech.ac.jp) and Mr Kawin SAIPRASERTKIT (saiprasertkit.k.aa@m.titech.ac.jp), Doctoral Candidate, are both in the Department of Civil Engineering, Tokyo Institute of Technology, Tokyo (Japan).